Determination of the α-Actinin–binding Site on Actin Filaments by Cryoelectron Microscopy and Image Analysis

Amy McGough, Michael Way,* and David DeRosier

Rosenstiel Basic Medical Sciences Research Center, Brandeis University, Waltham, Massachusetts 02254; and *Whitehead Institute for Biomedical Research, Cambridge, Massachusetts 02142

Abstract. The three-dimensional structure of actin filaments decorated with the actin-binding domain of chick smooth muscle α-actinin (αA1-2) has been determined to 21-Å resolution. The shape and location of αA1-2 was determined by subtracting maps of F-actin from the reconstruction of decorated filaments. αA1-2 resembles a bell that measures ~38 Å at its base and extends 42 Å from its base to its tip. In decorated filaments, the base of αA1-2 is centered about the outer face of subdomain 2 of actin and contacts subdomain 1 of two neighboring monomers along the long-pitch (two-start) helical strands. Using the atomic model of F-actin (Lorenz, M., D. Popp, and K. C. Holmes. 1993. *J. Mol. Biol.* 234:826–836.), we have been able to test directly the likelihood that specific actin residues, which have been previously identified by others, interact with αA1-2. Our results indicate that residues 86–117 and 350–375 comprise distinct binding sites for α-actinin on adjacent actin monomers.

T HE importance of actin in cellular processes ranging from muscle contraction to cell motility has made this protein one of the most widely studied since its discovery half a century ago (reviewed in Kabsch and Vandekerckhove, 1992). The function and dynamics of actin in the cell is regulated by a diverse group of proteins that bind either monomeric or filamentous actin or both (Pollard and Cooper, 1986; Vandekerckhove and Vancompernolle, 1992). α-Actinin is an F-actin cross-linking protein that is found in stress fibers and adhesion plaques in nonmuscle cells, as well as in Z discs and their homologues in muscle cells (Blanchard et al., 1989). Its function in the cell is not clear, but its subcellular distribution suggests that it may be important in the attachment of cytoskeletal structures to the membrane.

All α-actinin isoforms exist as homodimers of elongated subunits arranged in an antiparallel fashion. Each subunit is organized into domains: a 28-kD amino-terminal actin-binding domain (αA1-2)[1], four central α-helical repeats, and a carboxy-terminal domain containing two EF hand motifs (Baron et al., 1987). The actin-binding domain is related in sequence to similar-sized domains in dystrophin, spectrin, ABP120, filamin, and fimbrin (de Arruda et al., 1990; Matsudaira, 1991). Together, these proteins form a family of actin cross-linkers that differ primarily in the structure and number of central repeats. In addition, αA1-2 can functionally replace S2-3, an F-actin–binding domain in gelsolin that is unrelated in sequence but is of similar size (Way et al., 1992). Thus, the structure of αA1-2 is important as an archetype for the interactions of a number of proteins with actin filaments, including severing proteins such as gelsolin.

Monomer-binding proteins that block polymerization can be cocrystallized with G-actin and studied by x-ray crystallography (Kabsch et al., 1990; Schutt et al., 1993; McLaughlin et al., 1993). In the absence of such proteins, G-actin polymerizes into filaments, making crystals unattainable. Thus, electron microscopy is the method of choice for studying the structure of F-actin–binding proteins bound to actin filaments (Moore et al., 1970). Recent papers on myosin S1 interactions with F-actin demonstrate the power of combining the two approaches (Schroder et al., 1993; Rayment et al., 1993).

Current information about the location of α-actinin's binding site on actin has derived from a number of techniques including synthetic peptides, antibodies, affinity chromatography, and chemical cross-linking (Lebart et al., 1993, 1990; Mimura and Asano, 1987). With these methods, specific residues likely to be involved in binding have been identified, but structural information about the interaction is restricted to the interface between the proteins. We sought to determine directly the location of the binding site by electron microscopy and image processing of actin filaments decorated with αA1-2. The results show that αA1-2 contacts subdomain 1 of two actin monomers along the long-pitch helix of the filament at a site centered at subdomain 2.

Address all correspondence to Amy McGough, Rosenstiel Basic Medical Sciences Research Center, Brandeis University, 415 South Street, Waltham, MA 02254.

1. *Abbreviations used in this paper:* αA1-2, actin-binding domain of chick smooth muscle α-actinin; CTF, contrast transfer function.

Materials and Methods

Preparation of Decorated Filaments for Electron Microscopy

The actin-binding domain from chick smooth muscle α-actinin (residues 1–269) was expressed and purified from *Escherichia coli* as described previously (Way et al., 1992). G-actin was purified from chicken acetone powder by the method of Spudich and Watt (1971). Actin was polymerized in buffer A (10 mM Tris, pH 8, 100 mM NaCl, 1 mM MgCl$_2$, 0.2 mM ATP, 1 mM DTT, 3 mM NaN$_3$, 0.1 mM CaCl$_2$) for 30 min at room temperature. F-actin (0.05–1.0 mg/ml) in buffer A was incubated for 30 min at room temperature in the presence of a three- to sixfold molar excess of αA1-2. Reaction mixtures, pellets, and supernatants were analyzed by SDS-PAGE to determine the stoichiometry required for actin filament saturation (Way et al., 1992). We sought to reduce background noise in the micrographs by using the minimal amount of αA1-2 required to achieve saturation of the actin. Approximately 5 μl of filaments were applied to holey carbon copper electron microscope grids, blotted with filter paper, and rapidly frozen in liquid propane.

Electron Microscopy

Transmission electron microscopy was performed using an electron microscope (CM12; Philips Electronic Instruments, Inc., Mahwah, NJ) outfitted with an anticontaminator (651N; Gatan, Inc., Warrendale, PA). Electron microscope grids were maintained at $\sim -172\,^\circ$C using a cryotransfer system (626; Gatan, Inc.) cooled with liquid nitrogen. Images were recorded on film (SO-163; Eastman Kodak Co., Rochester, NY) at $\sim$1–1.2 μm under focus at a nominal magnification of 60,000 and an electron dose of $\sim$12 e$^-$/Å^2. Negatives were developed for 12 min in full-strength developer (D19; Eastman Kodak Co.).

Image Analysis

Three-dimensional reconstructions. Electron micrographs were digitized with a densitometer (1412; Eikonix Corp., Bedford, MA) at a scanning raster of 25 μm (resulting in a pixel size of $\sim$4.3 Å). Image analysis and display was performed on a Lexidata Lex 90 graphics device (Lexidata Corp., Billerica, MA) and a cluster of VAX workstations using a suite of programs written and maintained at Brandeis University. Filament images were straightened by fitting a spline to the particle axis and then interpolating onto a straight line (Egelman, 1986). Straightened images were masked and their edges were apodized before computing their Fourier transforms (Stewart et al., 1981). Approximate positions of the strongest layer-lines (typically 1, 2, 5, 6, and 7) were selected interactively. A least-squares fit of the strong reflections was used to determine the exact positions of all layer-lines in the Fourier transform (Owen and DeRosier, 1993). Layer-line data were collected within the first node of the transform, which was determined from regions of carbon support film adjacent to the particles analyzed.

After correcting for the phase origin and particle tilt, layer-lines were separated into near- and far-side data sets (DeRosier and Moore, 1970). We found that two rounds of interactive alignment were sufficient to align the data sets (Amos, 1975). Rotations and shifts were determined based on the phase minimum between each data set and a reference (using layer-lines 1, 2, 5, 6, and 7). In the first round, the reference was derived from one of the original images. In the second round, a preliminary average was used as the reference. A total of 80 data sets (from 40 filaments) were submitted for alignment. Of these, 12 were excluded because the polarities between the two sides of the same particle did not agree. The mean phase residual for the individual data sets against the reference (calculated using layer-lines 1, 2, 5, 6, and 7) was 72° and 61° for the first and last rounds of alignment, respectively. A phase residual of 61° is similar in magnitude to those reported for other actin structures such as F-actin decorated with Fab fragments, 53° (Orlova et al., 1994); actin-scruin filaments, 60° (Owen and DeRosier, 1993); and *Limulus* thin filaments, 54° (Lehman et al., 1994). Electron density maps were computed by Fourier-Bessel transformation of averaged layer-line data (DeRosier and Moore, 1970). The final reconstruction consisted of 68 data sets (from 34 filaments) corresponding to $\sim$3,800 subunits. Particle boundaries were determined based on the predicted volume of the filament using a protein density of 0.81 D/Å^3 and a molecular mass of 74 kD per unit cell.

Reliability of the map. We selected layer-lines to include in the reconstruction by determining the statistical significance of the Fourier

coefficients in the averaged data set, as described previously (Owen and DeRosier, 1993). 16 layer-lines contained significant data out to an approximate axial and radial resolution of 21 Å. Because the data were within the first node of the contrast transfer function (CTF), no phase corrections were necessary. Amplitude data at higher resolution in the Fourier transforms of the αA1-2–decorated filaments are attenuated by the CTF. This will result in a blurring of the subunits' boundaries but should not otherwise alter morphological features. There is no satisfactory way to correct this fall off for helical structures. Moreover, based on work done with S1-decorated actin, changes resulting from an uncorrected CTF do not appear to pose a problem (Milligan and Flicker, 1987). Therefore, we have chosen to present uncorrected data, as has been done by others (Owen and DeRosier, 1993; Unwin, 1993; Milligan et al., 1990). The significance of features within the reconstruction was determined by performing a Student's t test (Trachtenberg and DeRosier, 1987) for each pixel in the electron density map (two-sided, $n = 68$, $P = 0.95$). All features of the αA1-2–decorated filaments were significant by this criterion.

Comparison with other structures. The α-actinin portion of the reconstruction was identified by comparing the αA1-2–decorated filaments with other actin structures. This was done both qualitatively by inspection and, more quantitatively, by calculating difference maps. Three-dimensional reconstructions from electron micrographs of F-actin prepared under a number of conditions were kindly supplied by Edward Egelman (University of Minnesota, Minneapolis, MN) (Orlova and Egelman, 1992, 1993). Atomic models of actin (Holmes, 1990; Lorenz et al., 1993) were used to generate electron density maps of F-actin and then treated as electron microscopy data. All maps were brought to a common phase origin and rescaled to a common mean density before computing the differences. The expectation was that the positive density remaining after subtracting an F-actin map from the decorated filament would correspond to the αA1-2 fragment. This holds true assuming that the differences in the actin regions of the map are small, which is what we observed. The boundary of the fragment was chosen based on the predicted volume occupied by the actin-binding domain. Electron density maps and atomic models were displayed on a vector graphics device (PS300; Evans & Sutherland, Salt Lake City, UT) using the program FRODO (Jones, 1982).

Results

Appearance of αA1-2–decorated Filaments

Fig. 1 presents an electron micrograph of frozen-hydrated actin filaments decorated with αA1-2 (*a*) and the computed diffraction pattern (*c*) of one of the filaments (*b*). The low contrast in the images is caused by the absence of stain. The filaments are wider than undecorated F-actin. In the presence of the actin-binding domain of α-actinin, we found that short actin filaments were not uncommon. This observation supports the findings of Colombo and co-workers (1993), who found that α-actinin inhibits the annealing of F-actin after filament fragmentation. The modulation along the filaments arising from the twisting of the two long-pitch helices is more readily apparent in these decorated filaments than in naked F-actin. This is also evident in the computed diffraction patterns of decorated filaments in which the first three layer-lines, arising from the two-start helices, are intensified.

The Fourier transforms of decorated filaments show no significant deviations from the helical symmetry of F-actin. The mean symmetry for the 34 filaments included in the final reconstruction was 2.157 subunits/turn (SD = 0.0039). This means there are $\sim$28 subunits in 13 turns of the 59-Å "genetic" helix. The root-mean-squared angular deviation per subunit of the decorated filaments was calculated as described in Stokes and DeRosier (1987) and is $\sim$3.2° per subunit. This is somewhat less than the disorder measured for undecorated F-actin, 5.2° per subunit (Egelman and DeRosier, 1992). A decrease in the variability of actin's twist has also been observed in filaments decorated with myosin S1 and scruin (Stokes and DeRosier, 1987).
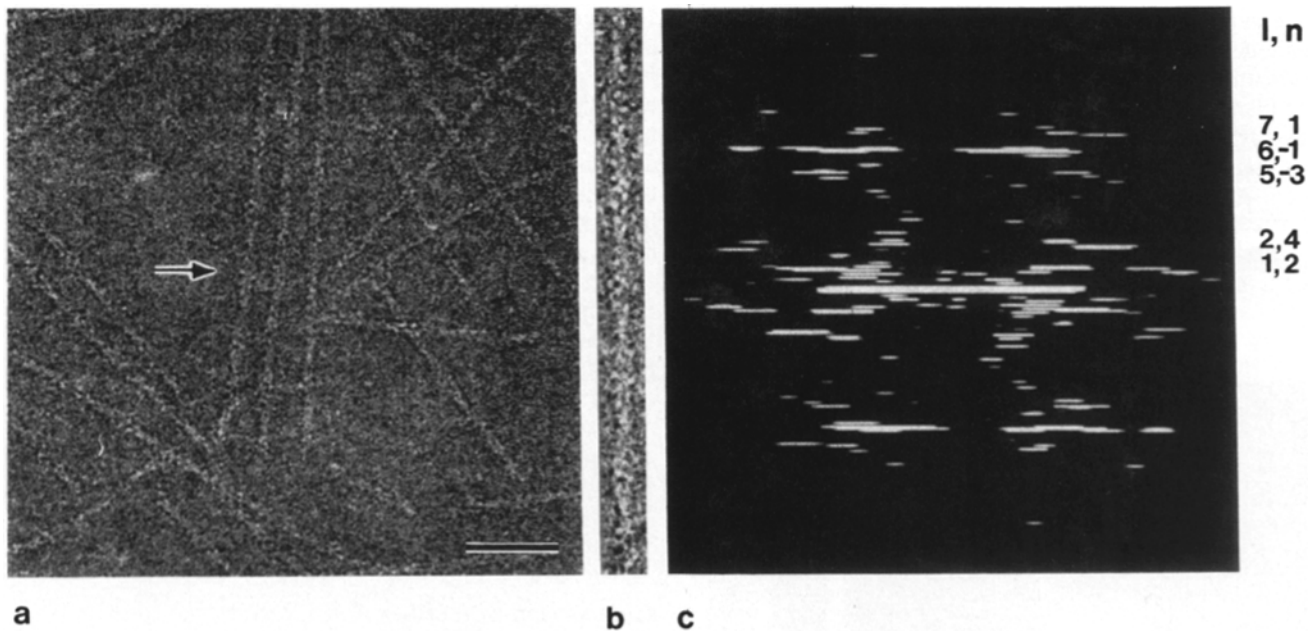
Figure 1. Actin filaments decorated with αAl-2. (*a*) Electron micrograph of αAl-2–decorated filaments preserved in vitreous ice. (*b*) 1.4 × enlargement of the filament that is indicated with an arrow in *a*. (*c*) Computed diffraction pattern of the filament shown in *b*. The number (*l*) and order (*n*) of the strong layer-lines are indicated. Bar, 500 Å.

To overcome the noise in the images, 34 filaments were aligned and averaged. Fig. 2 presents plots of amplitudes and phases for the averaged data set, the atomic model of F-actin (Lorenz et al., 1993), and a reconstruction of actin from

electron microscope data (Orlova and Egelman, 1992). The layer-line data for the αAl-2–decorated actin are very similar to that of other actin structures. The main differences between the αAl-2 decorated filaments and F-actin are an in-
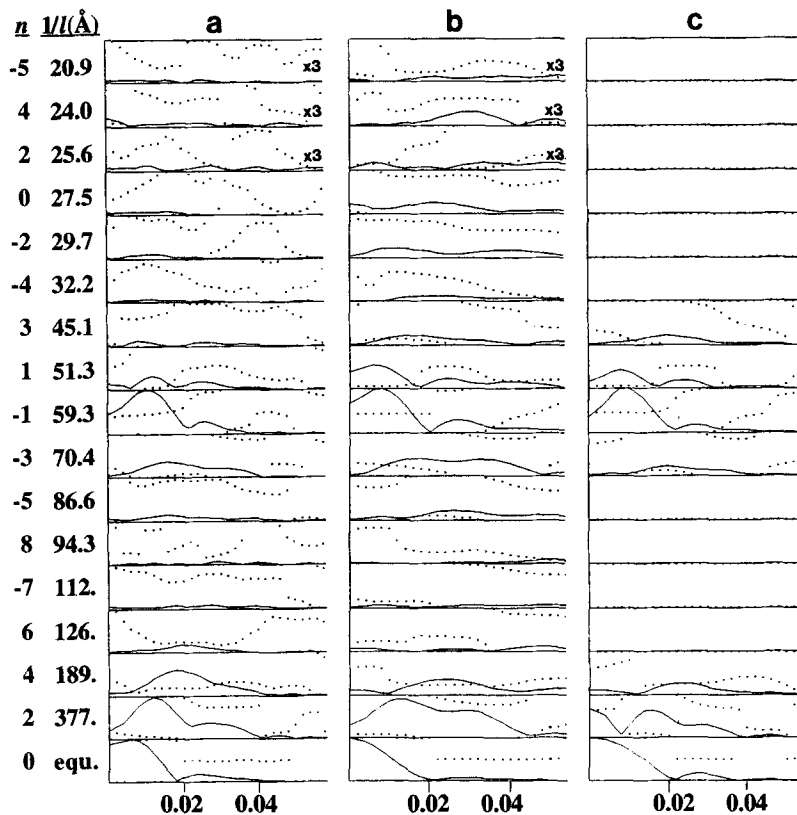

Figure 2. Plot of $G_{n,l}(R)$ (Klug et al., 1958) amplitudes (*solid curves*) and phases (*dotted curves*) for (*a*) αAl-2–decorated actin, (*b*) model F-actin (Lorenz et al., 1993), and (*c*) a reconstruction of F-actin prepared with beryllium fluoride from electron microscopy data (Orlova and Egelman, 1992). The order (*n*) and positions are listed for each layer-line. Amplitudes for the three highest layer-lines (25.6, 24.0, and 20.9) have been scaled 3×. Phases vary from 0° to 360°.

crease in the amplitudes of layer-lines 1–3, a decrease in the amplitudes on 7, and a shift of the peaks on layer-lines 1–3 towards the meridian relative to their positions in undecorated filaments. These differences are more readily apparent in the layer-line intensities of the computed diffraction patterns that are shown in Fig. 3, *a* and *c*.

Features in the Reconstructed Filaments

The three-dimensional reconstruction was generated by Fourier-Bessel inversion of the averaged layer-line dataset.
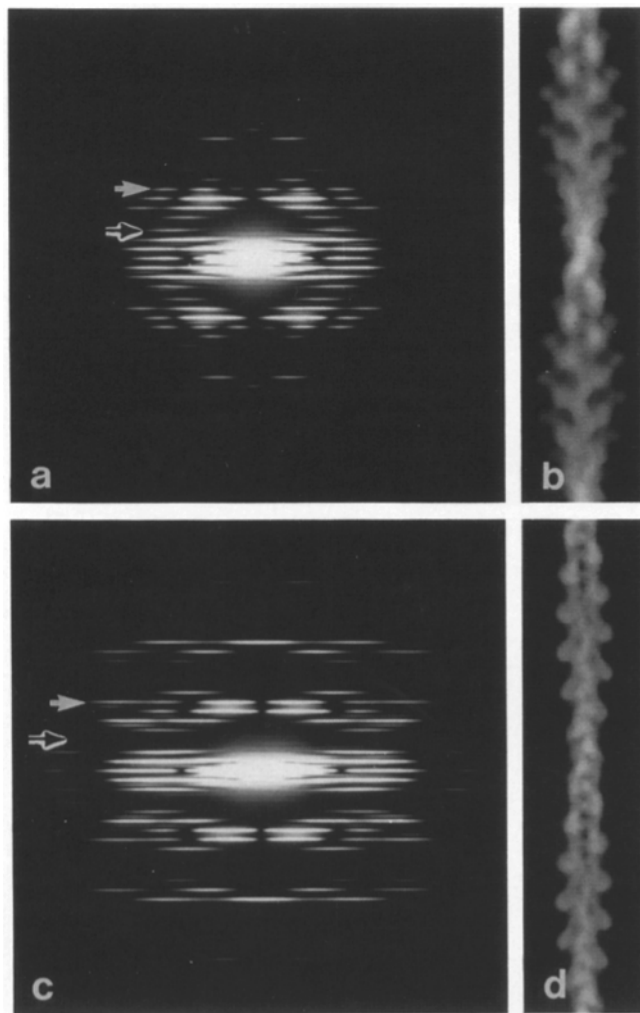

Figure 3. Diffraction pattern and projection image of (*a* and *b*) αAl-2–decorated actin and (*c* and *d*) model F-actin (Lorenz et al., 1993). The reconstruction of αAl-2–decorated actin is an average taken from 34 filaments. There is a dramatic improvement in the signal/noise ratio after averaging that can be readily seen by comparison with the images and diffraction patterns in Fig. 1 (*a* and *c*). The diffraction patterns show differences between decorated filaments and F-actin. The presence of the α-actinin fragment enhances the intensity of layer-line 3 (*hollow arrows*) and decreases the intensity of layer-line 7 (*solid arrows*) relative to undecorated actin. The peaks in the diffraction pattern of decorated filaments are shifted radially inward because of the increase in the diameter of these particles. (*b* and *d*) Projection images of the two structures show the presence of the actin-binding domain on decorated filaments. The αAl-2–decorated filaments are ~135 Å in diameter.

16 layer-lines plus the equator, extending out to a resolution of ~21 Å, were included at full weight in the reconstruction. Fig. 3 presents a projection image of the reconstructed filament (*b*) with F-actin (*d*) shown for comparison. Despite the presence of the 31-kD α-actinin actin-binding domain, the decorated filament still displays features characteristic of actin. The most obvious features are the two twisting long-pitch helices that are half-staggered relative to each other. The filaments differ because of the presence of extra density that increases the diameter to ~135 Å.

Comparison with other actin structures permitted us to assign the polarity of the component actin filament. The actin polarity is obvious on inspection, but it can be shown more rigorously by aligning the decorated filament with actin reconstructions. In all cases tested, the decorated filament gave an unambiguous result in the alignment. The up-down difference in phase residuals (calculated using layer-lines 1, 2, 5, 6, and 7) was typically ~25°. In Figs. 3, 5, and 6, the "pointed" or "minus" end of the actin filament is at the top.

Comparison with Other Actin Reconstructions

Fig. 4 presents sections through the reconstruction of αAl-2–decorated actin spaced 10 Å apart with a reconstruction of F-actin from electron microscopy data (Orlova and Egelman, 1992) and a model of the filament based on x-ray data (Lorenz et al., 1993). The outer contour of the map of the decorated filament was chosen to enclose a volume corresponding to actin plus αAl-2, but by inspection it is apparent that actin is overrepresented (Fig. 4 *a*). It roughly approximates the size of F-actin contoured at 135–145% of its calculated molecular volume. The contouring difficulties arise because the features corresponding to the αAl-2 are weaker than those of actin perhaps because of incomplete decoration. The actin maps presented in Fig. 4, *b* and *c*, have been contoured to match the volume of the actin portion of decorated filaments to aid in the comparison of the structures.

There is good agreement between the shapes and locations of the subdomains in the actin portion of the maps. Differences are restricted to the outer domain of actin (subdomains 1 and 2 according to the atomic model of the filament). In the first and third sections (at 0 and 20 Å), subdomain 1 is enlarged. However, there is no enlargement of subdomain 1 is the section cut at the approximate level of the amino terminus (30 Å). The clearest differences are seen in the section cut through subdomain 2 (10 Å), where αAl-2 is resolved into an additional distinct domain.

The shape of the α-actinin actin-binding domain was determined by subtracting F-actin from the entire reconstruction. Difference maps were computed using reconstructions of F-ADP-BeF$^-_3$ actin, lithium actin filaments, Ca^{2+}-Br^8-ATP actin filaments polymerized with KCl, F-Mg^{2+}-ADP filaments polymerized with Mg^{2+} from G-Mg^{2+}-ATP actin, and F-Mg^{2+}-ADP filaments polymerized with KCl from the G-Mg^{2+}-ATP actin (Orlova and Egelman, 1992; Orlova and Egelman, 1993) and with 20-Å resolution maps derived from two atomic models of F-actin (Holmes et al., 1990; Lorenz et al., 1993). Reconstructions were aligned in Fourier space and scaled to a common mean density in real space before subtracting one map from the other. There are slight variations in the domain's appearance depending on the actin structure used to calculate the difference map; however, the
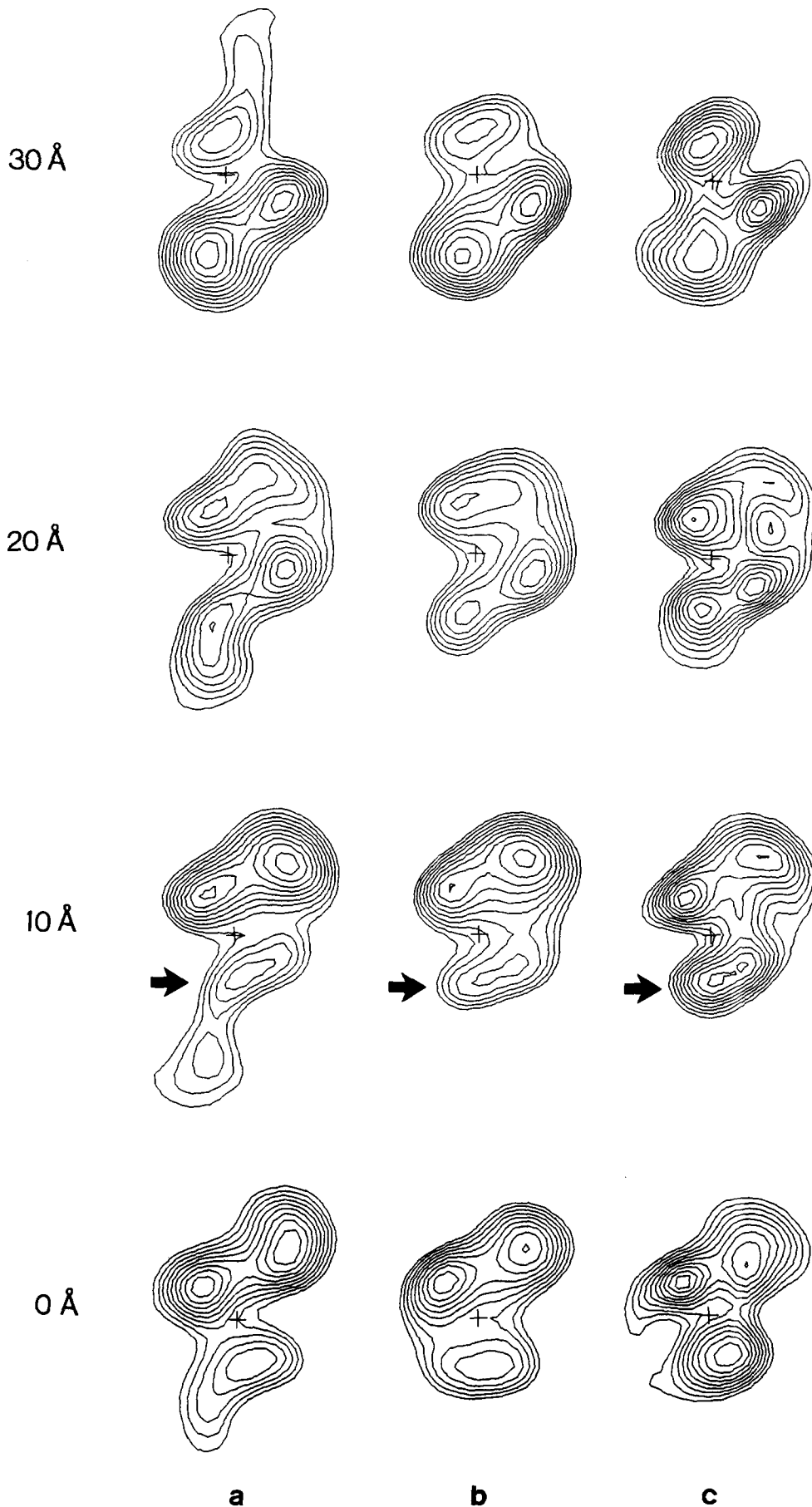
Figure 4. Comparison of actin structures in cross-section. (*a*) Sections, spaced ∼10 Å apart, through an αA1-2-decorated filament oriented with its pointed end down. The particle axis is indicated with a cross. Each section cuts through two different actin monomers in the filament, below and above the horizontal bar of the cross. Comparable sections through (*b*) a reconstruction of F-actin prepared with beryllium fluoride from electron microscopy data (Orlova and Egelman, 1992) and (*c*) a model fo the actin filament based on x-ray data (Lorenz et al., 1993) are shown contoured at 140% molecular volume for comparison purposes. In the second section (10 Å), subdomain 2 of the lower monomer is indicated with an arrow. The α-actinin domain is seen extending from subdomain 2 in this section. In the first (0 Å) and third (20 Å) sections, subdomain 1 is enlarged in the αA1-2-decorated filament. The fourth section (30 Å) is cut near the level of the amino terminus of the lower monomer. There is no evidence of αA1-2 density in this region of actin.
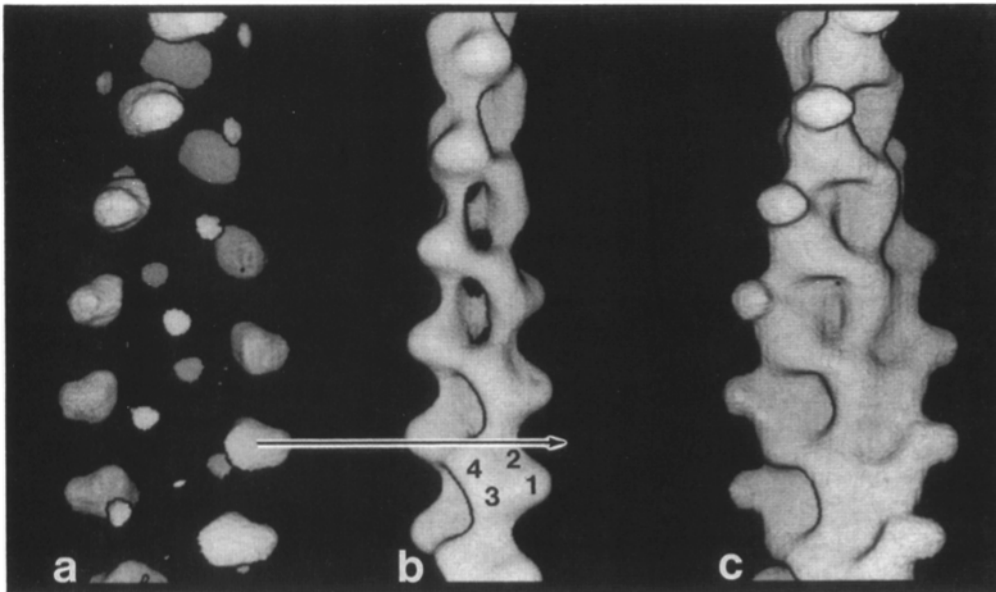
Figure 5. Positive density remaining after computing difference map. (*a*) Surface rendering showing the shape of the actin-binding domain determined by subtracting (*b*) F-ADP-BeF$^-_3$ actin (Orlova and Egelman, 1992) from (*c*) the αA1-2–decorated filament. The additional small mass present in the difference map is probably a result of imperfect density scaling of the maps before subtracting them. It falls outside the boundary of both actin and the αA1-2–decorated filament and is not significant according to the Student's *t* test calculated for the reconstruction. The approximate positions of the four subdomains of actin are indicated in *b*.

basic shape is the same. The best match in the actin portion of our map was to F-ADP-actin prepared in the presence of beryllium fluoride, therefore, these are the results that we present.

The positive density resulting from subtracting F-ADP-BeF$^-_3$ actin from the αA1-2–decorated filament structure is shown in Fig. 5. There are two peaks, but only one (the larger of the two) is significant according to the Student's *t* test. We interpret this as deriving from the αA1-2 fragment. The smaller peak is not significant and is located outside the boundary of both actin and the decorated filament.

The α-actinin domain resembles a bell or gumdrop with its base touching the actin filament. There is a small bump extending from the base that does not contact actin. The entire mass measures ∿38 Å at its base and extends 42 Å from its base to its tip. The actin-binding domain rests in the indentation between one monomer and the next one up the long-pitch strand. The binding site is centered around subdomain 2, but αA1-2 contacts portions of subdomain 1 of two different monomers. The base of αA1-2 forms an angle relative to the filament axis. This is most apparent in back views of the domain that are revealed as it follows the helical path of actin.

Discussion

Actin Structure

Recently, there have been several actin reconstructions done both in stain (Vibert et al., 1993; Owen and DeRosier, 1993; Egelman, 1986; Bremer et al., 1991) and in ice (Egelman, 1986; Schmid et al., 1994; Milligan et al., 1990). Both embedding methods give comparable structures to ⩾ 20 Å resolution. We compared our reconstruction to a number of other EM reconstructions of F-actin. In our reconstruction of αA1-2–decorated filaments, all four subdomains were readily identifiable. The actin portion of our map most closely matches that of F-ADP-actin prepared in beryllium fluoride (Orlova and Egelman, 1992), primarily because of

the position of subdomain 2. What is gratifying is that we see only one significant peak (presumably arising from the αA1-2 fragment) in the difference maps between our decorated filaments (in ice) and Orlova and Egelman's map of BeF actin (in stain). We also compared the αA1-2–decorated filaments with two atomic models of F-actin (Holmes et al., 1990; Lorenz et al., 1993). The major difference between these two models is in the positioning of subdomain 2, which is shifted towards the particle axis in the revised model. Actin filaments decorated with αA1-2 more closely resemble the revised model (Lorenz et al., 1993). In previously published EM reconstructions of F-ADP-actin subdomain 2 is not observed, presumably because of disorder in this domain (Milligan et al., 1990; Bremer et al., 1991; Orlova and Egelman, 1992). The fact that subdomain 2 is visible in our reconstruction suggests that its position is stabilized by interactions with αA1-2.

α-Actinin Actin-binding Domain Structure

Three-dimensional reconstructions obtained from two-dimensional crystals of α-actinin suggest that the actin-binding domain (αA1-2) consists of two ellipsoids of unequal sizes that form a "V" (Taylor, K., personal communication). The NH$_2$-terminal segment (αA1) is larger than the second segment (αA2) based on both the reconstruction and the predicted mass from the protein's sequence (de Arruda et al., 1990; Taylor and Taylor, 1993). In our reconstruction, we cannot resolve the two segments thought to comprise αA1-2. However, the bell-shaped appearance of the α-actinin portion of our map suggests that αA1-2 may consist of two or more subdomains. One interpretation of our reconstruction is that αA1 forms the base of the mass, touching actin, and αA2 corresponds to the smaller protrusion at the higher radius. This takes into account the evidence from a number of sources showing that the major portion of the actin-binding site is restricted to αA1 (Hemmings et al., 1992; Karinch et al., 1990; Levine et al., 1990, 1992; Way et al., 1992). Other interpretations are also possible. If the resolution is

sufficient, this domain assignment may be tested by fitting the αA1-2 portion of our reconstruction with the reconstruction of intact α-actinin.

It is also possible that there is a conformational change in αA1-2 upon binding actin that would lead to a difference in its appearance in our reconstruction relative to the structure of the unbound form. There is precedent for this notion. Wallraff et al. (1986) have observed a shortening of *Dictyostelium* α-actinin when bound by an antibody to the actin-binding site of the molecule. Meyer and Aebi (1990) found that some α-actinin isoforms shorten during bundle formation, raising the possibility that there is a conformational change in the molecule upon binding actin. Interestingly, this phenomenom was observed in *Acanthamoeba* and *Dictyostelium* α-actinin, but not in the chicken gizzard isoform. Nevertheless, a smaller conformational change might still exist in the smooth muscle α-actinin that does not produce a significant alteration in molecular length and, therefore, went undetected in their analysis.

α-Actinin Binding to Actin

Identification of the αA1-2–binding site by electron microscopy. Although at this resolution we cannot identify specific contacts between the α-actinin and actin molecules, there are regions of continuity between the two. We will refer to these as contacts as has been done by others (Milligan and Flicker, 1987; Owen and DeRosier, 1993). The αA1-2–binding site is centered at the front outer face of subdomain 2 of actin (Fig. 6, *a* and *b*). The lower half of the actin-binding domain rests on the front face of actin, whereas the upper portion is oriented more towards the back of actin. Because of its size, the actin-binding domain overlaps the top portion of subdomain 1 on the same monomer, as well as the bottom portion of the subdomain 1 on the next monomer up the two-start helix. The fact that the α-actinin domain contacts two actin monomers along the long-pitch helix may explain why it binds to F-actin but not to G-actin.

The geometry of αA1-2's interaction with a pair of actin subunits suggests a possible explanation for α-actinin's inability to nucleate polmerization. Compare this to gelsolin, which binds actin dimers and does nucleate polymerization (Doi and Frieden, 1984). Using chemically cross-linked actin, it has been shown that gelsolin binds two actin monomers that are "diagonally adjacent along the short-pitch helix of actin" (Doi, 1992). These and other observations have led to the assumption that the orientation of monomers in the gelsolin nucleator is across, rather than along, the actin filament (McLaughlin et al., 1993). In contrast, α-actinin binds two monomers along the long-pitch helix and does not nucleate polymerization.

α-Actinin–binding sites identified by other methods. A number of studies suggest that α-actinin binds to certain peptides in subdomain 1 of actin. Our reconstruction permits a direct test of the likelihood that the specific residues identified by others are involved in α-actinin binding. Fig. 6, *c* and *d*, presents the electron density map of αA1-2 with a carbon backbone rendering of actin. The putative binding sites are indicated on the actin model.

The 12 amino-terminal residues of actin were identified as a potential binding site by chemical cross-linking (Mimura and Asano, 1987). They do not appear to reside in the αA1-

2–binding site in our reconstruction. In support of this, antibodies directed against residues 1–7 of actin did not interfere with α-actinin binding (Lebart et al., 1993). Visual comparison of our reconstruction with one of filaments decorated with these antibodies (Orlova and Egelman, 1994) reveals that the sites are distinct. These residues are thought to be highly mobile (Kabsch et al., 1990). This may explain why they were detected by chemical cross-linking, but not in other assays.

Residues 86–117 (ABS1) and 350–375 (ABS2) have been identified as likely binding sites by a number of different techniques (Fabbrizio et al., 1993; Lebart et al., 1993, 1990; Mimura and Asano, 1987). These putative actin-binding sites, ABS1 and ABS2, have been highlighted in Fig. 6. The lower part of αA1-2 makes extensive contacts with the α helix at the interface between subdomains 1 and 2 (Trp 79–Asn 92). Weaker contacts are made between the top portion of α-actinin and subdomain 1 of the next actin monomer in the filament, in the region of Ser 350–Lys 359. This suggest that portions of ABS1 and ABS2 are contained in different α-actinin binding sites on adjacent actin monomers.

Recent mutational studies in yeast implicate both subdomain 1 and 2 in the binding site. SAC6 encodes the yeast form of fimbrin, a member of the α-actinin family of actin-binding proteins that contains two tandem αA1-2–like domains (Adams et al., 1989, 1991). Point mutations in yeast actin have been assessed for their ability to suppress the SAC6 mutant. All of the point mutants in actin that have been implicated in yeast fimbrin binding fall in either subdomain 2 or near the interface between subdomains 1 and 2 (Honts et al., 1994). Thus based on the sequence homology between α-actinin and fimbrin, we would expect the same residues in actin to be important for αA1-2 binding. This is consistent with our reconstruction. Site-directed changes in actin at position 99–100, when tested in yeast, produced phenotypes similar if not identical to SAC6 mutations, suggesting that these residues are involved in fimbrin binding (Holtzman et al., 1994). These two residues lie at the outside of subdomain 1, at or near the site of contact between actin and αA1-2, according to our reconstruction.

Relationship to Other F-Actin–binding Proteins

Myosin-binding site. From a structural standpoint, myosin is the best characterized of the F-actin binding proteins. There are now two models of its interactions with actin at atomic resolution that have been obtained by combining data from x-ray crystallography, fiber diffraction, and electron microscopy (Schroder et al., 1993; Rayment et al., 1993). The primary contacts made by myosin are on the outer face of subdomain 1, with additional sites on subdomain 3. There are also minor contacts on the outer domain of an adjacent monomer (Milligan et al., 1990). Myosin S1 and α-actinin do not appear to compete for the same site on immobilized monomeric actin (Lebart et al., 1993). This is consistent with our reconstruction, which shows that the α-actinin binding site is centered on subdomain 2.

Tropomyosin-binding site. Electron microscopy and image analysis have been used to identify tropomyosin's binding site(s) on actin filaments (Milligan and Flicker, 1987; Milligan et al., 1990; Vibert et al., 1993; Lehman et al., 1994). Skeletal muscle tropomyosin is found on the "inner domain"
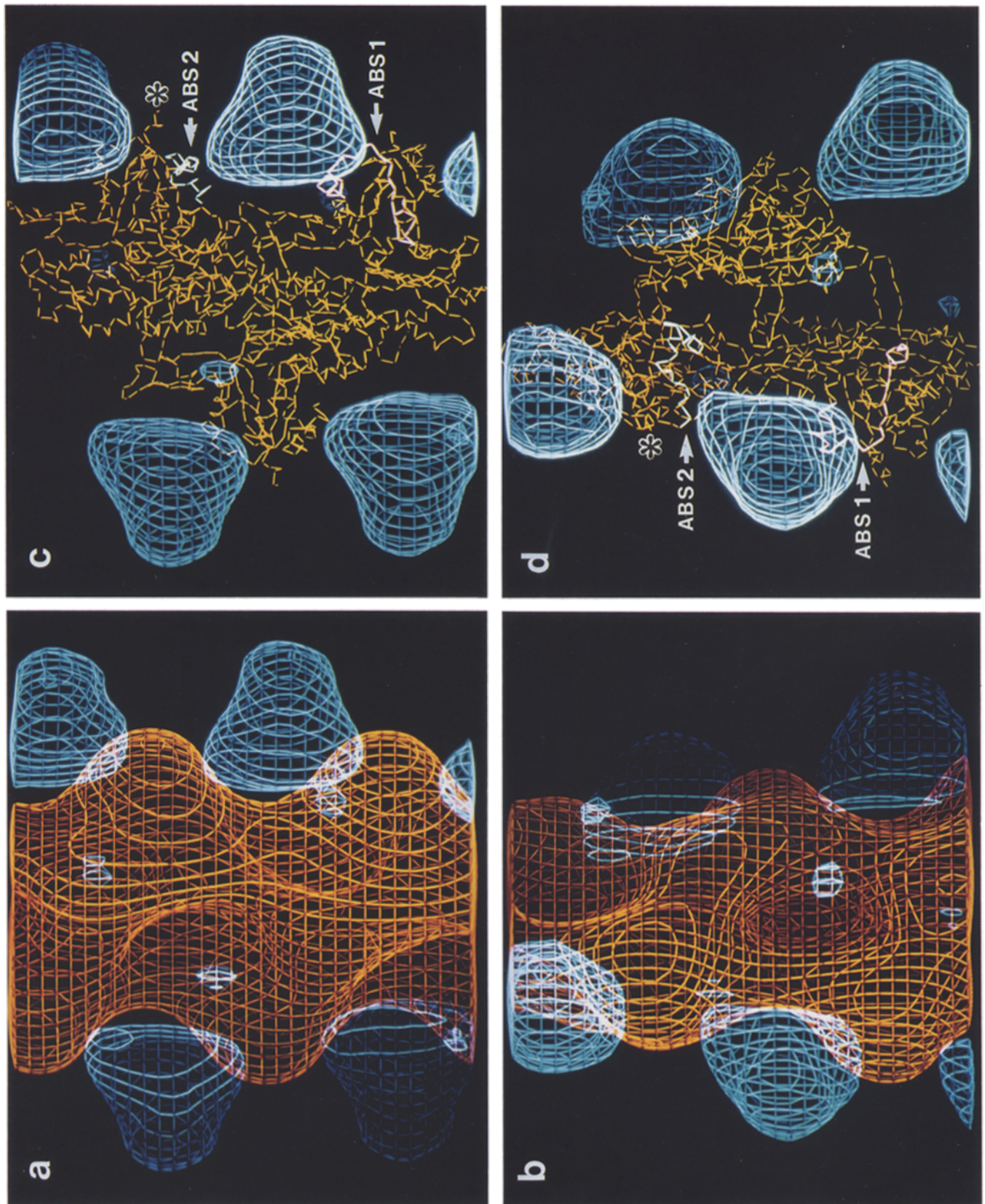
Figure 6. Location of the alpha-actinin binding site on actin. (*a* and *b*) The electron density arising from αA1-2 (*blue*) shown with the F-ADP-BeF$^-_3$ actin reconstruction (*orange*; Orlova and Egelman, 1992) used to compute the difference map. The structures have been rotated clockwise ~135° in *b*. (*c* and *d*) The αA1-2 electron density shown with the atomic model of F-actin (Lorenz et al., 1993). Three actin monomers are shown in yellow. ABS1 (86-117) and ABS2 (350-375) are highlighted in pink and green. The position of the amino terminus of the top monomer is indicated with an asterisk.

in the presence of calcium (Vibert and Craig, 1982; Milligan and Flicker, 1987; Milligan et al., 1990; Lehman et al., 1994). In the absence of calcium, tropomyosin is shifted towards and makes contacts with the outer domain of actin, near the junction between subdomains 1 and 3 (Lehman et al., 1994). Interestingly, the situation appears to be reversed in smooth muscle, where the regulatory function of troponin is replaced by caldesmon (Vibert et al., 1993). Thus, tropomyosin appears to be in a position to sterically inhibit α-actinin binding in the "off" state of skeletal muscle and in the "on" state of smooth muscle. In vitro studies have shown that tropomyosin can compete with α-actinin for actin binding (Goll et al., 1972; Zeece et al., 1979; Grazi et al., 1991). This raises the possibility that tropomyosin is at least partly responsible for determining the distribution of α-actinin–containing structures (Z bands, dense bodies) in muscle cells.

Scruin-binding site. Scruin is a 102-kD protein that is present in the acrosomal process of *Limulus* sperm (Tilney, 1975). It contains a duplicated actin-binding domain that is found in a number of proteins, including the *Drosophila* protein kelch (Way, M., and P. Matsudaira, manuscript in preparation). Scruin crosslinks actin filaments into a highly ordered bundle (Schmid et al., 1993). Three-dimensional reconstructions from electron micrographs of filaments (Owen and DeRosier, 1993) and bundles (Schmid et al., 1994) show the interactions of these two proteins at 13-Å resolution, making this by far the best-characterized actin-binding protein by electron microscopy.

In contrast to α-actinin, scruin contacts two actin monomers across the genetic helix of actin. One domain of scruin contacts one monomer on its front face (relative to the orientation of G-actin in Kabsch et al. [1990]) at subdomain 1 and at the junction between subdomains 3 and 4. The other domain of scruin binds the second actin monomer on the back face of subdomains 1 and 2. This would appear to leave the outer regions of subdomains 1 and 2 available for interaction with α-actinin (see Fig. 4, *d* and *f*; Owen and DeRosier, 1993).

Implications for the Severing Mechanism of Gelsolin

Gelsolin is a calcium-regulated actin severing protein with homologies to fragmin, severin, and villin (Way and Weeds, 1988). It is organized into six repeats, termed S1-6, whose different activities have been partially characterized (reviewed in Janmey, 1993; Weeds and Maciver, 1993). The monomer binding sites are located in S1 and S4-6 (Bryan, 1988; Yin et al., 1988; Way et al., 1989), and the F-actin binding site is in S2 (Way et al., 1992). Efficient severing and barbed end capping require segments 1 and 2 of gelsolin (Way et al., 1992).

Recently, the structure of gelsolin S1 in complex with G-actin was solved by x-ray crystallography (McLaughlin et al., 1993). Segment 1 is tightly bound in the cleft between subdomains 1 and 3 in a site that would correspond to the barbed end of the actin filament. Based on some of the binding properties of the individual domains and sequence similarities between segments, McLaughlin et al. (1993) proposed a model for gelsolin binding to F-actin and filament capping. According to the model, S1 and S4 bind to the same site on adjacent actin monomers across the genetic helix (see Fig. 4 *a*; McLaughlin et al., 1993). This dictates that segments 2 and 3 connect the two domains by running across

the filament by the shortest route, bringing it in contact with the inner domain of actin (see Fig. 4 *c*; McLaughlin et al., 1993). Based on our structure and available data, we suggest that an alternative model is required.

Way et al. (1992) have proposed that the F-actin binding domain of α-actinin is functionally analogous to S2-3 based on the following observations: the F-actin–binding domains of gelsolin (S2-3) and α-actinin (αA1-2) compete for the same binding site on filaments in vitro and a hybrid protein comprised of segment 1 of gelsolin and the actin-binding domain of α-actinin was found to have similar severing activities to gelsolin S1-3. This implies that αA1-2 positions gelsolin segment 1 correctly for severing and must have a similar binding site to that of S2-3. The logical conclusion from this suggestion is that the F-actin binding domain of gelsolin (S2-3) binds to the outer domain of actin in a similar position to that of αA1-2 in our reconstruction. This position is inconsistent with the model of McLaughlin et al. (1993) and is more consistent with an earlier model proposed by Pope et al. (1991), in which S2-3 binds on the outer domain of actin at the interface between two monomers on the long-pitch helix of the filament.

Conclusions

The actin-binding domain of α-actinin is an archetype for related domains in a large number of actin crosslinking proteins, including dystrophin and fimbrin. Previous studies had localized the α-actinin binding site to primarily two sites on actin, at residues 86–117 and 350–375 (Fabbrizio et al., 1993; Lebart et al., 1993, 1990; Mimura and Asano, 1987). Because both sites fall on subdomain 1 of actin, the simplest interpretation of the data available at the time was that α-actinin binds to a single monomer. Using electron microscopy and image processing, we have found that αA1-2 actually contacts two monomers along the long-pitch helix of the actin filament at a site centered at subdomain 2. This structure provides a framework for understanding numerous biochemical data on the properties of α-actinin, including its specificity for filamentous versus monomeric actin, its inability to nucleate actin polymerization, and the competition by tropomyosin for actin binding. In addition, the agreement between our structure and the SAC6 studies in yeast provide support for the view that the actin-binding domains of fimbrin and α-actinin are in fact homologues. Finally, this structure also provides important insights into how severing proteins such as gelsolin bind actin filaments to sever them.

References

Adams, A. E. M., D. Botstein, and D. G. Drubin. 1989. A yeast actin-binding protein is encoded by SAC6, a gene found by suppression of an actin mutation. *Science (Wash. DC).* 243:231–233.

Adams, A. E. M., D. Botstein, and D. G. Drubin. 1991. Requirement of yeast fimbrin for actin organization and morphogenesis in vivo. *Nature (Lond.).* 354:404–408.

Amos, L. A. 1975. Combination of data from helical particles: correlation and selection. *J. Mol. Biol.* 99:65–73.

Baron, M. D., M. D. Davison, P. Jones, and D. R. Critchley. 1987. The sequence of chick alpha-actinin reveals homologies to spectrin and calmodulin. *J. Biol. Chem.* 262:17623–17629.

Blanchard, A., V. Ohanian, and D. Critchley. 1989. The structure and function of α-actinin. *J. Musc. Res. Cell Motil.* 10:280–289.

Bremer, A., R. C. Millonig, R. Sutterlin, A. Engel, T. D. Pollard, and U. Aebi. 1991. The structural basis for the intrinsic disorder to the actin filament: the "lateral slipping" model. *J. Cell Biol.* 115:689–703.

Bryan, J. 1988. Gelsolin has three actin-binding sites. *J. Cell Biol.* 106:1553–1562.

Colombo, R., I. DalleDonne, and A. Milzani. 1993. Alpha-actinin increases actin filament end concentration by inhibiting annealing. *J. Mol. Biol.* 230:1151–1158.

de Arruda, M. V., S. Watson, C.-S. Lin, J. Leavitt, and P. Matsudaira. 1990. Fimbrin is a homologue of the cytoplasmic phosphoprotein plastin and has domains homologous with calmodulin and actin gelation proteins. *J. Cell Biol.* 111:1069–1079.

DeRosier, D. J., and P. B. Moore. 1970. Reconstruction of three-dimensional images from electron micrographs of structures with helical symmetry. *J. Mol. Biol.* 52:355–369.

Doi, Y., and C. Frieden. 1984. Actin polymerization. The effect of brevin on filament size and rate of polymerization. *J. Biol. Chem.* 259:11868–11875.

Doi, Y. 1992. Interaction of gelsolin with covalently cross-linked actin dimer. *Biochemistry.* 31:10061–10069.

Egelman, E. H. 1986. An algorithm for straightening images of curved filamentous structures. *Ultramicroscopy.* 19:367–374.

Egelman, E. H., and D. J. DeRosier. 1992. Image analysis shows that variations in actin crossover spacing are random, not compensatory. *Biophys. J.* 63:1299–1305.

Fabbrizio, E., A. Bonet-Kerrache, J. J. Leger, and D. Mornet. 1993. Actin-dystrophin interface. *Biochemistry.* 32:10457–10463.

Goll, D. E., A. Suzuki, J. Temple, and G. R. Holmes. 1972. Studies on purified α-actinin. I. Effect of temperature and tropomyosin on the α-actinin/F-actin interaction. *J. Mol. Biol.* 67:469–488.

Grazi, E., G. Trombetta, and M. Guidoboni. 1991. Binding of α-actinin to F-actin or to tropomyosin F-actin is a function of both α-actinin concentration and gel structure. *J. Mucle Res. Cell Motil.* 12:579–584.

Hemmings, L., P. A. Kuhlman, and D. Critchley. 1992. Analysis of the actin-binding domain of α-actinin by mutagenesis and demonstration that dystrophin contains a functionally homologous domain. *J. Cell Biol.* 116:1360–1380.

Holmes, K. C., D. Popp, W. Gebhard, and W. Kabsch. 1990. Atomic model of the actin filament. *Nature (Lond.).* 347:44–49.

Holtzman, D., K. Wertman, and D. Drubin. 1994. Mapping actin surfaces required for functional interactions in vivo. *J. Cell Biol.* 126:423–432.

Honts, J. E., T. S. Sandrock, S. M. Brower, J. L. O'Dell, and A. E. M. Adams. 1994. Actin mutations that suppress and are suppressed by fimbrin mutations identify a likely fimbrin-binding site on actin. *J. Cell Biol.* 126:413–422.

Janmey, P. 1993. A slice of the actin. *Nature (Lond.).* 364:675–676.

Jones, T. A. 1982. FRODO: A graphics fitting program for macromolecules. *In* Computational Crystallography. D. Sayre, editor. Claredon Press, Oxford. p. 303–317.

Kabsch, W., H. G. Mannherz, D. Suck, E. F. Pai, and K. C. Holmes. 1990. Atomic structure of the actin: DNase I complex. *Nature (Lond.).* 347:37–44.

Kabsch, W., and J. Vandekerckhove. 1992. Structure and function of actin. *Annu. Rev. Biophys. Biomol. Struct.* 21:49–76.

Karinch A. M., W. E. Zimmer, and S. R. Goodman. 1990. The identification and sequence of the actin-binding domain of human red blood cell beta-spectrin. *J. Biol. Chem.* 265:11833–11840.

Klug, A., F. H. C. Crick, and H. W. Wycoff. 1958. Diffraction by helical structures. *Acta Crystallogr.* 11:199–213.

Lebart, M.-C., C. Mejean, M. Boyer, C. Roustan, and Y. Benyamin. 1990. Localization of a new alpha-actinin binding site on the COOH-terminal part of the actin sequence. *Biochem. Biophys. Res. Commun.* 173:120–126.

Lebart, M.-C., C. Mejean, C. Roustan, and Y. Benyamin. 1993. Further characterization of the alpha-actinin-actin interface and comparison with filamin-binding sites. *J. Biol. Chem.* 268:5642–5648.

Lehman, W., R. Craig, and P. Vibert. 1994. Ca⁺⁺-induced tropomyosin movement in *Limulus* thin filaments revealed by three-dimensional reconstruction. *Nature (Lond.).* 368:65–67.

Levine, B. A., A. J. G. Moir, V. B. Patchell, and S. V. Perry. 1990. The interaction of actin with dystrophin. *FEBS (Fed. Eur. Biochem. Soc.) Lett.* 262:159–162.

Levine, B. A., A. J. G. Moir, V. B. Patchell, and S. V. Perry. 1992. Binding sites involved in the interaction of actin with the N-terminal region of dystro-

phin. *FEBS (Fed. Eur. Biochem. Soc.) Lett.* 298:44–48.

Lorenz, M., D. Popp, and K. C. Holmes. 1993. Refinement of the F-actin model against fiber diffraction data by the use of a directed mutation algorithm. *J. Mol. Biol.* 234:826–836.

Matsudaira, P. 1991. Modular organization of actin crosslinking proteins. *Trends Biochem. Sci.* 16:87–92.

McLaughlin, P. J., J. T. Gooch, H.-G. Mannherz, and A. G. Weeds. 1993. Structure of gelsolin segment 1-actin complex and the mechanism of filament severing. *Nature (Lond.).* 364:685–692.

Meyer, R. K., and U. Aebi. 1990. Bundling of actin filaments by α-actinin depends on its molecular length. *J. Cell Biol.* 110:2013–2024.

Milligan, R. A., M. Whittaker, and D. Safer. 1990. Molecular structure of F-actin and location of surface binding sites. *Nature (Lond.).* 348:217–221.

Milligan, R. A., and P. F. Flicker. 1987. Structural relationships of actin, myosin, and tropomyosin revealed by cryo-electron microscopy. *J. Cell Biol.* 105:29–39.

Mimura, N., and A. Asano. 1987. Further characterization of a conserved actin-binding 27-kDa fragment of actinogelin and alpha-actinins and mapping of their binding sites on the actin molecule by chemical cross-linking. *J. Biol. Chem.* 262:4717–4723.

Moore, P. B., H. E. Huxley, and D. J. DeRosier. 1970. Three-dimensional reconstructions of F-actin, thin filaments and decorated thin filaments. *J. Mol. Biol.* 50:279–295.

Owen, C., and D. DeRosier. 1993. A 13-Å map of the actin-scruin filaments from the *Limulus* acrosomal process. *J. Cell Biol.* 123:337–344.

Orlova, A., and E. H. Egelman. 1992. Structural basis for the destabilization of F-actin by phosphate release following ATP hydrolysis. *J. Mol. Biol.* 227:1043–1053.

Orlova, A., and E. H. Egelman. 1993. A conformation change in the actin subunit can change the flexibility of the actin filament. *J. Mol. Biol.* 232:334–341.

Orlova, A., X. Yu, and E. H. Egelman. 1994. Three-dimensional reconstruction of a co-complex of F-actin with antibody Fab fragments to actin's NH₂ terminus. *Biophys. J.* 66:276–285.

Pollard, T. D., and J. A. Cooper. 1986. Actin and actin-binding proteins. A critical evaluation of mechanisms and functions. *Annu. Rev. Biochem.* 55:987–1035.

Pope, B., M. Way, and A. G. Weeds. 1991. Two of the three actin-binding domains of gelsolin bind to the same subdomain of actin: implications for capping and severing mechanisms. *FEBS (Fed. Eur. Biochem. Soc.) Lett.* 280:70–74.

Rayment, I., H. M. Holden, and M. Whittaker, C. B. Yohn, M. Lorenz, K. C. Holmes, and R. A. Milligan. 1993. Structure of the actin-myosin complex and its implications for muscle contraction. *Science (Wash. DC).* 261:58–65.

Schmid, M. F., J. Agris, J. Jakana, P. Matsudaira, and W. Chiu. 1994. Three-dimensional structure of a single filament in the *Limulus* acrosomal bundle: scruin binds to homologous helix-loop-beta motifs in actin. 1991. *J. Cell Biol.* 124:341–350.

Schmid, M. F., J. Jakana, P. Matsudaira, and W. Chiu. 1993. Imaging frozen, hydrated acrosomal bundle from Limulus sperm at 7 Å resolution with a 400 KV electron cryomicroscope. *J. Mol. Biol.* 230:384–386.

Schroder, R. R., D. J. Manstein, W. Jahn, H. Holden, I. Rayment, K. C. Holmes, and J. A. Spudich. 1993. Three-dimensional atomic model of F-actin decorated with *Dictyostelium* myosin S1. *Nature (Lond.).* 364:171–174.

Schutt, C. E., J. Myslik, M. D. Rozycki, N. C. W. Gonnesekere, and U. Lindberg. 1993. The structure of crystalline profilin-β-actin. *Nature (Lond.).* 365:810–816.

Spudich, J. A., and S. Watt. 1971. The regulation of rabbit skeletal muscle contraction. I. Biochemical studies of the interaction of the tropomyosin-troponin complex with actin and the proteolytic fragments of myosin. *J. Biol. Chem.* 246:4866–4871.

Stewart, M., R. W. Kensler, and R. J. C. Levine. 1981. Structure of *Limulus* telson muscle thick filaments. *J. Mol. Biol.* 153:781–790.

Stokes, D. L., and D. J. DeRosier. 1987. The variable twist of actin and its modulation by actin-binding proteins. *J. Cell Biol.* 104:1005–1017.

Taylor, K. A., and D. W. Taylor. 1993. Projection image of smooth muscle alpha-actinin from two-dimensional crystals formed on positively charged lipid layers. *J. Mol. Biol.* 230:196–205.

Tilney, L. G. 1975. Actin filaments in the acrosomal reaction of *Limulus* sperm. *J. Cell Biol.* 64:289–310.

Trachtenberg, S., and D. J. DeRosier. 1987. Three-dimensional structure of the frozen-hydrated flagellar filament: the left-handed filament of *Salmonella typhimurium. J. Mol. Biol.* 195:581–601.

Unwin, N. 1993. Nicotinic acetylcholine receptor at 9 Å resolution. *J. Mol. Biol.* 229:1101–1124.

Vandekerckhove, J., and K. Vancompernolle. 1992. Structural relationships of actin-binding proteins. *Curr. Opin. Cell Biol.* 4:36–42.

Vibert, P. V., and R. Craig. 1982. Three-dimensional reconstruction of thin filaments decorated with a Ca²⁺-regulated myosin. *J. Mol. Biol.* 157:299–319.

Vibert, P. V., R. Craig, and W. Lehman. 1993. Three-dimensional reconstruction of caldesmon-containing smooth muscle thin filaments. *J. Cell Biol.* 123:313–321.

Wallraff, E., M. Schleicher, M. Modersitzki, D. Rieger, G. Isenberg, and G.

Gerisch. 1986. Selection of Dictyostelium mutants defective in cytoskeletal proteins: use of an antibody that binds to the ends of α-actinin rods. *EMBO (Eur. Mol. Biol. Organ.) J.* 5:61–67.

Way, M., J. Gooch, B. Pope, and A. G. Weeds. 1989. Expression of human plasma gelsolin in Escherichia coli and dissection of actin binding sites by segmental deletion mutagenesis. *J. Cell Biol.* 109:593–605.

Way, M., B. Pope, and A. G. Weeds. 1992. Evidence of functional homology in the F-actin–binding domains of gelsolin and α-actinin: implications for the requirements of severing and capping. *J. Cell Biol.* 119:835–842.

Way, M., and A. G. Weeds. 1988. Nucleotide sequence of pig plasma gelsolin. Comparison of protein sequence with human gelsolin and other actin-severing proteins shows strong homologies and evidence for large internal repeats. *J. Mol. Biol.* 203:1127–1133.

Weeds, A. G., and S. Maciver. 1993. F-actin capping proteins. *Curr. Opin. Cell Biol.* 119:835–842.

Yin, H. L., K. Iida, and P. A. Janmey. 1988. Identification of a polyphospho-inositide-modulated domain in gelsolin which binds to the sides of actin filaments. *J. Cell Biol.* 106:805–812.

Zeece, M. G., R. M. Robinson, and P. J. Bechtel. 1979. Interaction of α-actinin, filamin, and tropomyosin with F-actin. *Biochim. Biophys. Acta.* 581: 365–370.